

## Effect of wind variability and variable air density on wave modeling

Saleh Abdalla

European Centre for Medium-Range Weather Forecasts, Reading, UK

Luigi Cavaleri

Istituto Studio Dinamica Grandi Masse, Venice, Italy

Received 14 September 2000; revised 19 December 2001; accepted 27 December 2001; published 25 July 2002.

[1] The impact of wind gustiness on the evolution of wave fields is analyzed by superimposing to the nominal wind speed a fluctuation whose amplitude is related to the local air-sea temperature difference. The use of fluctuations represented by a Gaussian process, characterized by coherence in time, produces realistic time series whose characteristics are compatible with those obtained from previous studies and open sea measurements. For the sake of forcing a wave model two more representations of gustiness have been used, a simple alternate oscillation of fixed amplitude around the mean value and a Gaussian process without coherence in time. The introduction of gustiness leads to an evident average increase of the resulting wave heights, larger in the Atlantic Ocean than in the Mediterranean Sea. The randomness of the wind and, hence, to a more limited extent, of the wave fields implies the possible occurrence of wave heights much larger than expected in a nongusty field. Besides two 6 month hindcasts two ensemble exercises have been done by forcing two storms with 50 different random realizations of the input wind fields. On the basis of the statistics of the outputs the authors suggest for practical applications the use of two runs, without and with noncoherent gustiness. This will provide information on the statistics of the possible significant wave heights. The effect of a variable air density on wave generation has been explored by repeating the hindcasts using air density values estimated from the output of a meteorological model. It is found that in the North Atlantic Ocean this leads to an increase of the wave heights during the winter storms. The effects are more limited in the Mediterranean Sea. *INDEX TERMS*: 3379 Meteorology and Atmospheric Dynamics: Turbulence; 4247 Oceanography: General: Marine meteorology; 4255 Oceanography: General: Numerical modeling; 4504 Oceanography: Physical: Air/sea interactions (0312); 4560 Oceanography: Physical: Surface waves and tides (1255); *KEYWORDS*: wind waves, wind, gustiness, wave growth, wave modeling, air density

### 1. Introduction

[2] Wind-wave modeling has reached a rather satisfactory level for practical applications with the development of the third-generation wave models [e.g., *Komen et al.*, 1994]. At the same time the progressive improvement in meteorological modeling, and, in particular, in the description of the surface wind fields has led to the gradual decrease of errors experienced in the past decade [see, e.g., *Jacob et al.*, 2000; *Bidlot et al.*, 2000].

[3] The reduction of the bias in the analysis, when compared to the measured data, is not reflected in a comparable reduction of the root mean square error. The reason for this is associated with the intrinsic variability of the atmosphere, also at the smaller scales, not sufficiently represented in the present meteorological models [see

*Simmons*, 1991; *Cavaleri et al.*, 1997]. Of course, the consequences are felt also in all the applications using the wind fields as input. Wave modeling is an obvious example.

[4] The variability of the atmosphere is present basically at all the scales, from microturbulence, passing through the synoptic level, duly represented in the meteorological models, and above. The basic question we face in this paper is how to estimate the implications of these oscillations, which we will refer to as gustiness, for the evaluation of wind waves in the oceans.

[5] There have been a few attempts to introduce gustiness into practical use. *Cavaleri and Burgers* [1992] used sequences of random numbers, normalized in amplitude and correlated in time, to simulate the time series recorded at open sea stations. This technique, once applied to real storms [*Komen et al.*, 1994, pp. 326–329], led to an improvement of the model results. However, the level of gustiness was not objectively determined and taken as

constant in space and time. *Ponce and Ocampo-Torres* [1998] explored the sensitivity of a wave model to wind variability. In particular, they used an extended series of high-frequency wind measurements in the Gulf of California to estimate the variability to be added to the output fields of a meteorological model. They found an induced increase of the resulting wave heights and a broadening of the directional spectra.

[6] *Bauer and Weisse* [2000] followed a rather sophisticated approach, using empirical orthogonal functions to derive a numerical representation of gustiness from a long-term record of wind speed in the open sea. They were quite successful in reproducing the gustiness spectrum and went on applying it to a winter hindcast in the North Atlantic Ocean. The results indicated a mild, but clear, increase of the significant wave heights. However, the significance of their results is somehow limited by the use of a gustiness that was numerically sophisticated but uniform in space and time. As a matter of fact, the level of gustiness can change dramatically, depending on the characteristics of the atmosphere and the ocean. One example is given by *Komen et al.* [1994, p. 271].

[7] The main aim of this paper is to explore, in a more complete and comprehensive way, the implications of gustiness for wave modeling, both in idealized cases and in practical applications. In so doing we will implicitly assume, as all the quoted previous attempts, that the wind is constant during each integration time step of the model. The implications of neglecting the higher-frequency wind oscillations will be discussed in section 8.

[8] Besides wind speed the momentum (and energy) transfer from air to sea depends also on the air density. This dependence is included in wave models via the wind input source term. However, the wave models usually assume a constant air density ( $\rho_a \approx 1.225 \text{ kg m}^{-3}$ ) throughout. The second aim of this work is to introduce the estimated correct value of the air density in the wave model we used and to analyze the implications for the derived wave fields.

[9] The paper is organized as follows. Section 2 describes briefly the wave model used for the tests, focusing on the parts that are related to the present discussions. Section 3 includes some discussion on wind gustiness and a description of the approach followed for its simulation. Furthermore, the consequences on wave growth are discussed. Section 4 further elaborates these consequences, where the response of an infinite uniform ocean to a gusty wind is analyzed. Getting rid of all the complications of a real ocean, this is useful to understanding the response of the wave system and the reasons for the different behaviors. Section 5, with this background, describes the applications to the real ocean with two extensive hindcasts carried out in an enclosed basin and in an open ocean.

[10] The implication of using a variable air density, as derived from an operational meteorological model, instead of an assumed constant average value, as is traditionally done, is the theme of the next part of the paper. Section 6 is dedicated to representing those implications for idealized cases, as was done for the gustiness. Section 7 repeats the hindcast applications presented in the previous sections, with a variable air density. Then section 8 discusses the

different findings, their limitations and their implications. Finally, section 9 summarizes the conclusions.

## 2. WAM Model

[11] The WAM wave model [*WAMDI Group*, 1988; *Komen et al.*, 1994] was used for the tests. The model integrates, numerically, the wave action balance equation using an explicit scheme for the advection terms and a semi-implicit scheme for the source function terms. The source function consists of terms accounting for wind input [*Miles*, 1957; *Janssen*, 1991], nonlinear wave-wave interaction [*Hasselmann*, 1962; *Hasselmann et al.*, 1985], and wave dissipation due to white capping [*Hasselmann*, 1974; *Komen et al.*, 1984; *Janssen et al.*, 1989] in addition to other terms to account for processes in finite water depths, when applicable. *Komen et al.* [1994] provide a thorough description of the model. Attention here will be concentrated on the wind input source term where the wind gustiness and air density come into the picture within the wave modeling.

[12] On the basis of a quasi-linear assumption, *Miles* [1957] proposed a theoretical expression to estimate the rate of energy transfer from a steady and uniform wind field to waves as follows:

$$\frac{\partial F}{\partial t} = \gamma F, \quad (1)$$

where  $F$  is the spectral energy,  $t$  is the time, and  $\gamma$  is the growth rate, which is [see, e.g., *Snyder et al.*, 1981] proportional with the air-water density ratio  $\rho_a / \rho_w$  (where  $\rho_a$  and  $\rho_w$  are the air and the water densities, respectively) and with the difference,  $U \cos \phi - c$ , between the wind velocity component in the along-wave direction and the wave phase velocity  $c$  (where  $\phi$  is the angle between wind and wave propagation directions). Expression (1) is valid for each component of the wave spectrum, specified in frequency and direction. Later experimental studies showed that  $\gamma$  as can be inferred directly from Miles formulations is lower than the measured growth rates. More appropriate expressions for  $\gamma$  were proposed by several researchers, such as *Snyder et al.* [1981] and *Komen et al.* [1984]. *Janssen et al.* [1989] further modified the expression by taking into consideration the wave-induced stress, then incorporated in the latest version of WAM model cycle 4 [*Janssen*, 1991].

[13] One can find from the theory [see, e.g., *Snyder et al.*, 1981] that energy transfer from wind to waves occurs when the wind (component) moves faster than the waves,  $U \cos \phi - c > 0$ . For wind slower than the phase speed of the waves,  $U \cos \phi - c < 0$ , there is no energy transfer to either side. There is some criticism of the latter statement, and indeed, some theories [e.g., *Makin and Kudryavtsev*, 1999] suggest that some energy transfer does occur also from waves to wind. However, the corresponding wave decay rates according to these theories are very low compared to the growth rates. Therefore neglecting this transfer does not have in any case appreciable consequences on the conclusions of this work.

[14] Cycle 4 of the WAM model was used for all the tests presented here. The modifications made were limited to the

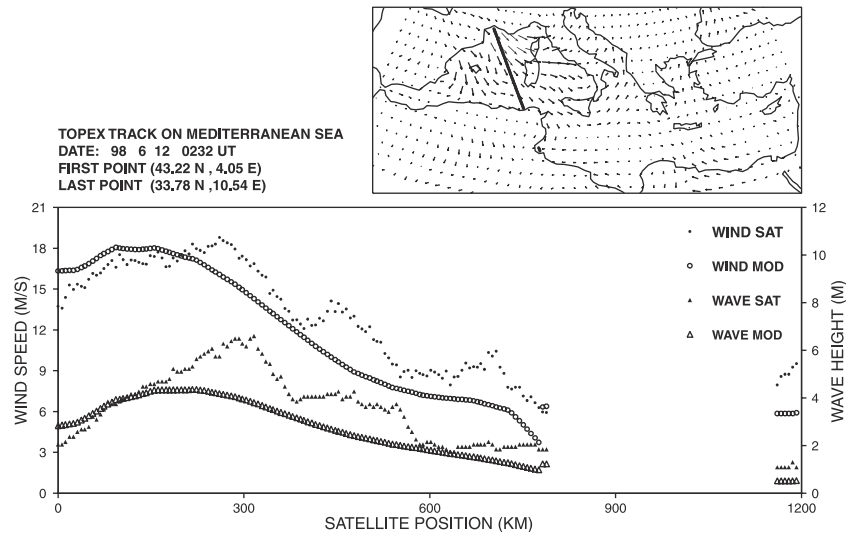


**Figure 1.** Comparison between model and TOPEX altimeter-measured wind speeds and significant wave heights during a Mistral storm in the western Mediterranean Sea. The thick line in the small map shows the satellite ground track.

aspects of concern for this study. At each grid point and time step the wave conditions are specified by a two-dimensional spectrum defined by 25 frequency components and 12 directional bins. At each time step this spectrum can be integrated to get the one-dimensional spectrum and integral wave parameters, such as the significant wave height  $H_s$ , the mean and peak periods,  $T_m$  and  $T_p$ , the mean wave direction  $\theta_m$ , and the total and wave stresses,  $\tau$  and  $\tau_w$ . The integration time step  $\Delta t$ , both for the advection scheme and for the integration of source terms, was taken as 15 or 20 min, depending on the spatial grid size. Initial conditions were used as a standard mean Joint North Sea Wave Project (JONSWAP) spectrum [Hasselmann *et al.*, 1973] with  $H_s = 0.36$  m and a  $\cos^2$  spreading function.

[15] The single-point version of the model, used for the idealized cases, was obtained by limiting the basin to only one grid point and by dropping out the advection terms. This corresponds to assuming an infinite ocean with spatially homogeneous conditions and only temporal variability.

### 3. Wind Gustiness

#### 3.1. Wind Gustiness in Wave Modeling

[16] There is a fair amount of information on the variability of the atmosphere at the different scales. A general description of the characteristics of surface winds on the oceans has been given by Freilich and Chelton [1986] and Tournadre and Blanquet [1994]. On the basis of satellite data their analysis could not consider the lower range of the scale, being limited to 200 and 20 km, respectively. This range has been more commonly explored in time using in situ wind measurements. Several dedicated experiments were conducted to study the small-scale characteristics, for example, Humidity Exchange Over the Sea program (HEXOS) [Smith *et al.*, 1990].

[17] Most of this wealth of information on wind gustiness has not yet found its way to wave modeling. There are several reasons behind this. First of all, apart from dedicated

cases the information available from the meteorological models comes typically at 3 or, mostly, 6 hour intervals. This puts an immediate lower limit on the scales of wind variability one can objectively have at one's disposal. Besides, most meteorological models introduce for numerical stability reasons some numerical diffusion in the lower layers, which tends to smear further the finest details of the field [see Simmons, 1991; Cavaleri *et al.*, 1997]. Finally, the theory itself cannot explain the large level of gustiness found under certain conditions in the measured data (A. Beljaars, personal communication, 2000) [see also Panofsky and Dutton, 1984]. We want to stress that apart from the practicality for operational applications, high-resolution modeling in space and time is not necessarily a solution as part of the above limitations still hold.

[18] For our present interests it seems therefore that the level of wind variability present in the atmosphere is partially filtered in the available meteorological model data. The level of filtering depends on the wavelength, increasing toward its lower values and, for wave hindcast purposes, having a drastic cutoff established by the frequency of archiving. A good example is given in Figure 1, where altimeter-estimated wind and wave data are compared with the corresponding model output for a Mistral storm in the western Mediterranean Sea. It is clear that the measured field exhibits oscillations at different scales not reproduced in the model output, the dominant one being, in this case, between 200 and 300 km wavelength.

[19] One way to overcome the above limitations for wave modeling is to superimpose on the input wind fields some numerical variability with characteristics consistent with the available theoretical and experimental information and the specific conditions at the spot, in space and time, under consideration. Our first task is the determination of a suitable algorithm for the numerical representation of gustiness.

[20] General information on the spectra of surface winds is well documented in the literature. Freilich and Chelton

[1986] analyzed scatterometer data in the Northern and Southern Hemispheres and found the wave number dependence of the kinetic energy spectrum to be  $k^{-2.2}$  and  $k^{-1.9}$ , respectively. *Tournadre and Blanquet* [1994] analyzed both spatial (satellite altimeter) and temporal (platform anemometers) data and found the spectral slope, in wave number and frequency space, to be similarly close to  $-1.8$ . We have analyzed extensive records from several stations in the North Atlantic and found the slope to be  $-1.7$  on the average.

[21] There is ample evidence [e.g., *Munn, 1966; Smith et al., 1990*] that the fluctuations of wind speed and direction around an average value are well represented by a Gaussian distribution. A straightforward application of these results is the superposition on the mean wind of a Gaussian signal with the correct level of variability.

[22] The superposition of a simple Gaussian noise on the model wind data would produce an unrealistic rather white spectrum. One way to avoid this is to introduce a correlation between the sequential data at a given location. This barely reflects the physical evidence that sequential speed values are not independent but tend to hover around a gradually varying mean. Therefore, following *Cavaleri and Burgers* [1992], for the purpose of this study the wind speed fluctuations were simulated according to

$$b_i = \alpha b_{i-1} + a_i, \quad (2)$$

where  $b$  is the sought sequence,  $a$  is a sequence of random numbers with a Gaussian distribution of zero mean and unity variance,  $\alpha$  is the coherence coefficient with values between 0 and 1, and the subscript denotes rank in the sequence. Expression (2) represents an autoregressive process of first order, and with the proper choice of  $\alpha$  leads to realistic time sequences with spectral characteristics that are consistent with the real wind spectra, as discussed above. We have analyzed the wind records at our disposal (mainly North Atlantic records) and found on average  $\alpha = 0.9$ . The sequences produced using this value in equation (2) have a spectral shape in good agreement with the real ones. Minor modifications of  $\alpha$ , for example,  $\pm 0.05$ , would cause significant deviations from the realistic spectra. The standard deviation of the constructed sequence  $\sigma_b$  is related to the standard deviation of the random sequence  $\sigma_a$  as [*Box and Jenkins, 1970*]

$$\sigma_a^2 = (1 - \alpha^2)\sigma_b^2. \quad (3)$$

[23] We are still left with the determination of the value of  $\sigma$  (defined hereafter as the normalized standard deviation by the mean value) under given conditions using the data available in practical applications. According to present theory [e.g., *Panofsky and Dutton, 1984*],  $\sigma$  can reach values close to 10%. However, much larger values of gustiness are possible in nature, as reported by, for example, *Monahan and Armendariz* [1971] and *Sethuraman* [1979]. The North Atlantic wind records we analyzed indicated the existence of  $\sigma$  values in excess of 30%. Similar values were derived also from the records obtained from the oceanographic tower of the Istituto Studio Dinamica Grandi Masse (ISDGM) [*Cavaleri, 2000*]. To our best

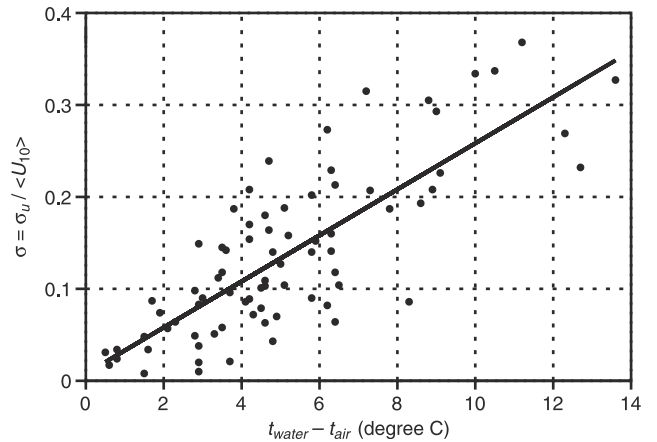


**Figure 2.** The correlation between  $\sigma$ , the standard deviation of wind speed normalized by its mean speed value, and the difference between water and air temperatures.

knowledge, literature only provides expressions relating the  $\sigma$  level to the inversion height and the Monin-Obukhov length [e.g., *Panofsky and Dutton, 1984*]. Determination of such parameters is not straightforward, if at all possible outside a meteorological model, from the standard archived data.

[24] If the theory does not provide the values of gustiness we find in nature, we should look for a more pragmatic approach. Physical background and experimental evidence suggest that the amplitudes of the oscillations depend somehow on the wind speed and on the stability conditions of the lower atmosphere. A characterization of the stability can be obtained from the air-sea temperature difference. As these parameters are regularly available from the operational meteorological models, this seems a convenient approach to the problem. On the basis of the wind velocity, air temperature, and water temperature records obtained at the ISDGM tower a relationship has been found (see Figure 2) between the standard deviation of wind speed normalized with respect to the mean speed value,  $\sigma = \sigma_u / \langle U_{10} \rangle$ , and the difference  $\Delta T$  between sea and air temperature, in degree Celsius. Each dot in Figure 2 represents a record of 1 hour duration. Only positive  $\Delta T$  were considered here, with  $\langle U_{10} \rangle$  larger than  $5 \text{ m s}^{-1}$ . For negative  $\Delta T$  there is always a minimum level of gustiness, but limited to a few percent, too low to influence appreciably the wave growth [see *Komen et al., 1994, p. 322*]. Within the scatter of the data the best fit line to the data suggests with good approximation

$$\sigma = \max [0., 0.025(T_{\text{water}} - T_{\text{air}})], \quad (4)$$

with  $T_{\text{water}}$  and  $T_{\text{air}}$  being the water and air temperatures, measured at  $-5$  and  $21$  m, respectively, with respect to the mean sea level. Lacking other sources of information, we have therefore resorted to the use of equation (4).

[25] Coherence in time, as expressed by equation (2), implies also coherence in space. The general view of gustiness superimposed to a constant and uniform wind field can be compared to a wavy surface, with the single oscillation propagating mainly along the wind direction.

The practical problem is the quantification of the coherence in space. *Tournadre and Blanquet* [1994] provide estimates of spectra down to the scale of 20 km. However, their data have been filtered to eliminate the high-frequency oscillations. An estimate can be obtained considering the advection of turbulence by the wind field [*Panofsky and Dutton*, 1984]. Starting from the coherence in time, and assuming a mean wind speed of, for example,  $15 \text{ m s}^{-1}$ , this suggests a comparable coherence in space at distances on the order of 10 km. The grid resolution of the wave model dictates the significance of the spatial coherence. As is better explained later in section 5, we used for our tests the resolutions of  $0.25$  and  $1^\circ$ . While for the lower limit the coherence between adjacent grid points may still be significant, this is not the case for the upper limit. To carry out all the tests in a consistent manner, we have decided to neglect the spatial coherence, which is consistent with the assumption of *Bauer and Weisse* [2000]. Therefore the time series derived from equation (2) will be evaluated independently for each grid point. The implications of this choice will be discussed in section 8.

[26] Besides wind speed we considered the oscillations of wind direction. We found that with the exception of rather low and sparse winds, its fluctuations are rather small and almost independent on the air-sea stability conditions and the level of gustiness of wind speed. For wind speeds larger than  $5 \text{ m s}^{-1}$  the standard deviation of the wind direction fluctuations was found to have a  $4^\circ$  mean value and a maximum not exceeding  $10^\circ$ . For the simulation a procedure similar to the one for wind speed was followed.

### 3.2. Structure of Numerical Simulations

[27] The overall procedure to estimate the wind gustiness for wave modeling is therefore the following. We derive from the meteorological archive the distribution, in time and space, of surface wind speed ( $U_{10}$ ),  $T_{\text{waters}}$  and  $T_{\text{air}}$ . For each synoptic time when this information is available (for the European Centre for Medium-Range Weather Forecasts (ECMWF), 0000, 0600, 1200, and 1800 UTC) and for each grid point we derive from equation (4) the corresponding  $\sigma_b$  value, which leads, through equation (3), to the corresponding  $\sigma_a$  value. At each wave model integration time step the  $U_{10}$  and  $\sigma_a$  fields are interpolated between the bordering synoptic times. The  $b$  sequence is constructed using expression (2) and the appropriate  $\alpha$  value (0.9). Multiplied by the interpolated  $\sigma_a$  and  $U_{10}$  values, its superposition to the interpolated  $U_{10}$  value itself provides the input wind time series to the wave model.

[28] This procedure provides quasi-realistic sequences of wind speed. While they are suitable for realistic hindcasts, the complex pattern of the fields and the different processes at work hide the pure effect of gustiness. For a proper understanding of its implications it is convenient to carry out first some simplified tests. Therefore gustiness is simulated in three different ways for the purpose of this study.

1. The variable  $a$  in equation (2) is forced to take alternatively the values  $+1$  and  $-1$ , and  $\alpha$  is set equal to 0. This results in a flip-flop fluctuation that simulates wind gustiness, discarding both the randomness and the coherence of the phenomenon. On the other hand, this provides a clear picture about the pure effect of wind oscillations. Runs

with this type of simulation will be termed hereafter as flip-flop runs.

2. The variable  $a$  is obtained using a random number generator and follows the Gaussian distribution with zero mean and unity variance. Here  $\alpha$  is set equal to 0. This results in a random fluctuation that simulates wind gustiness, discarding its coherence in time. Although this does not represent a realistic gusty wind, it is used to assess, by comparison, the importance of the coherence in the simulations. Runs with this type of simulation will be termed hereafter as the no-coherence runs.

3. The variable  $a$  is obtained as in the no-coherence case, but  $\alpha = 0.9$ . This results in a more realistic representation of wind gustiness. Runs with this type of simulation will be termed hereafter as coherence runs.

### 3.3. Effect on Wave Growth

[29] Three mechanisms lead to an enhancement of the wave field in the presence of gustiness, sorted with the more significant one at the top:

1. As mentioned above, wind is only able to input energy to waves with phase velocity lower than the wind velocity. For a well-developed sea, when part of the components in the spectrum have a phase speed larger than the mean wind speed, the excess of energy transferred to the wave spectrum due to an increase of wind speed is not compensated by a corresponding decrease during the opposite phase. This leads to a net positive increase in the energy pumped to the waves in the presence of gustiness compared to a steady wind with the same mean wind speed. Because of the analogy with the filtering capability of an electronic diode, we term this mechanism as diode effect.

2. According to various studies [see, e.g., *Smith et al.*, 1990] the variations in the surface wind speed  $U_{10}$  are Gaussian distributed. The wave generation mechanism is a function of the friction velocity  $u_*$ , which is nonlinear (grows faster) with respect to  $U_{10}$ . Therefore the mean  $u_*$  is greater than the value of  $u_*$  corresponding to the mean  $U_{10}$ .

3. According to the *Janssen* [1991] formulation the input to waves has a rather concave dependence on  $u_*$ . This enhances slightly the effect of gustiness.

[30] While mechanisms 2 and 3 are active throughout the process, the first one becomes effective only at an advanced stage of development, when energy is present also in the sufficiently low frequency, hence fast, wave components. Therefore a gusty wind results in marginal enhancement of wave growth at the early stages of development, significant differences being expected only at a later stage.

## 4. Single-Point Gustiness Runs

[31] Because of the complication of the natural conditions, it is convenient to begin the tests with some idealized conditions. The single-point version of the WAM model was used for this purpose. The single-point runs were carried out using the standard WAM model cycle 4 [see *Komen et al.*, 1994], limited to a basin of a single computational point with the propagation terms switched off. A mean wind speed of  $15 \text{ m s}^{-1}$  was used for all the single-point runs presented here. Other wind speeds were used, but are not presented, as the results are fully consistent with those reported here. The wind gustiness was simulated

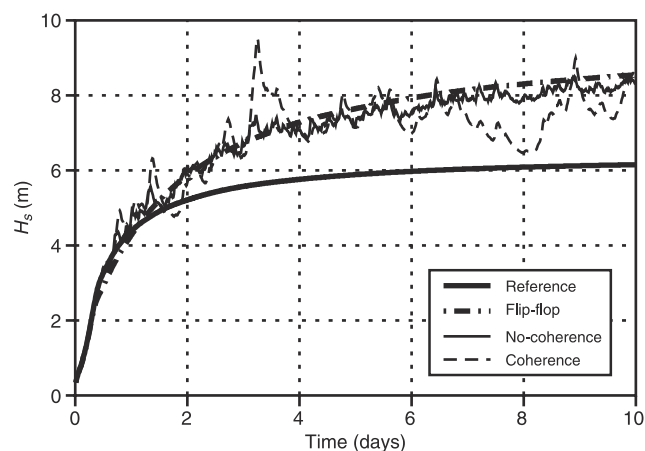


**Figure 3.** Effect of wind gustiness on the significant wave height growth curves from single-point runs with a standard integration time step.

using predetermined  $\sigma$  values. The three types of numerical gustiness, namely, flip-flop, no-coherence, and coherence, were used. Wind direction was kept constant throughout these runs.

[32] A reference run was carried out using a steady wind speed of  $15 \text{ m s}^{-1}$ . Various runs with different levels of gustiness were carried out, but only the results obtained with  $\sigma = 0.25$  are presented. Apart from the magnitude of the impact, all the other results are consistent with what is reported here.

[33] The significant wave height growth curves of the gusty tests are compared to the reference run in Figure 3. Gustiness has almost no effect on the wave growth during the very early stages. The increase in wave height during the mature and late stages of development is significant, around 1 m or about 20% increase after 3 days of simulation. It is interesting to note that the gusty curve keeps growing in time, without an evident tendency to approach a limiting value, even after 10 or (not shown) 30 days of simulations. The reason for this is that at any stage, there are in the spectrum wave components with phase speed close to the wind one, hence suitable for the diode effect.

[34] A notable fact, of relevance for the practical applications, is that during the second half of the first day of simulation the gusty wind results in lower wave heights compared to the nongusty curve. This is termed hereafter as the kink in the growth curve. This kink turned out to be attributed to the response of the numerical scheme used for the integration of the source terms in the WAM model under rapidly varying wind speeds. We found also that this kink is responsible for wave height underestimation for fetch-limited conditions as waves are mainly in the developing stage. Several numerical tests showed that using smaller integration time steps (not exceeding 3 min) would eliminate most of the kink. This problem was touched on, and a solution was proposed by *Hersbach and Janssen* [1999].

[35] The no-coherence growth curve has limited oscillations associated with randomness, and on the average it differs only slightly from the corresponding smooth flip-flop curve. The coherence curve shows large random oscillations of different periods. It is important to realize

that these oscillations, introduced in the time series because of the coherence, are significant only from a statistical point of view. Only the average values (in a certain period) and the amplitude of the oscillations can be compared. For a better understanding of their statistical properties the ensemble technique has been used. The test was repeated 100 times with different random number sequences, and both the average and the envelope of the 100 growth curves are presented in Figure 4, together with the growth curves corresponding to the reference and flip-flop runs. The flip-flop growth curve coincides, more or less, with the mean of the 100 coherence gusty runs. An analysis of the statistical distribution of the  $H_s$  values suggested that the normalized standard deviation of significant wave height,  $\sigma_{H_s}/H_s$ , is a function of the stage of wave development. It increases abruptly during the early stages of development, then starts to decrease till the later stages. In absolute terms the wave height variability grows very rapidly during the first day, after which, its maximum remains more or less constant.

[36] To examine the implications of wind direction variability on wave modeling, several tests were carried out following the general path as with wind speed. Those tests indicated that introducing random variations of wind direction with standard deviation of  $10^\circ$ , which is the upper limit observed, would lead to a reduction of the significant wave height by about 1% compared to the reference run (not shown). Therefore it was decided to neglect the effect of the directional variations by not introducing them into further simulations.

## 5. Practical Applications With Gustiness

[37] To assess the possible effects of the wind gustiness on wave growth under practical conditions, two long-term hindcast experiments were conducted. The first was a 6 month, winter 1993–1994, continuous wave hindcast study in the Mediterranean Sea to reflect the effect of gustiness under relatively short fetch conditions. The other experiment was another 6 month, winter 1999–2000, hind-

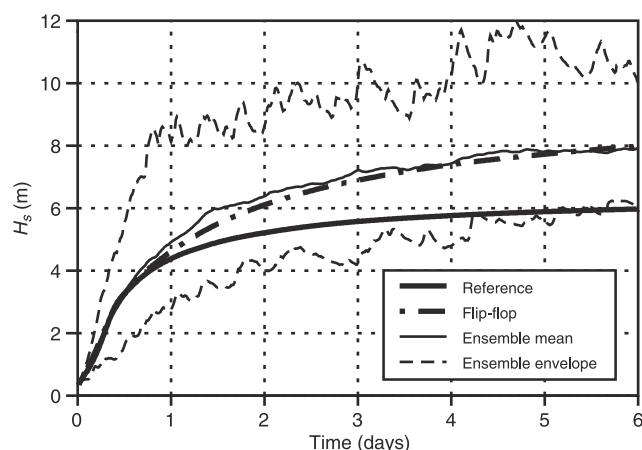


**Figure 4.** The mean and the envelope of the growth curves resulting from 100 coherence runs with different random number sequences. The reference and the flip-flop curves are given for comparison.

**Table 1.** Results of the Tests in the Mediterranean Sea<sup>a</sup>

	MR	MF	MN	MC15	MC03	MD
Maximum negative difference, m	...	-0.58	-0.75	-1.59	-1.41	-0.37
Lowest mean, m	1.44	-0.02	-0.01	-0.01	-0.00	-0.01
Highest mean, m	1.44	+0.00	+0.00	+0.02	+0.03	+0.01
Maximum positive difference, m	9.57	+0.24	+0.64	+1.58	+2.01	0.33

<sup>a</sup>The first row provides the maximum negative difference, in space and time, with respect to the reference run MR. The second row refers to the longterm average differences on the single points of the grid. The third and fourth rows provide the corresponding positive results. The first column shows the overall mean and maximum for the MR run. MF is flip-flop run, MN is the random run without coherence, MC15 is the random run with coherence, MC03 is similar to MC15 but with an integration time step of 3 min, MD is the run with actual air density.

cast study in the North Atlantic to explore the possible effects under long fetch conditions.

[38] Before reporting the results of the tests and the comparison with the available measurements it is important to stress that with the introduction of gustiness any such comparison can be done only from a statistical point of view. Any realization of a gusty sequence obtained using equation (2) is just one of the many possible cases. Even if the physical assumptions underlying equations (2), (3), and (4) are correct, it is most likely that a given time sequence has little to do with what has really happened in nature, except in statistical terms.

[39] Another point to stress is that while we are convinced that the introduction of gustiness and the use of a variable air density are steps in the right direction, we do not expect this will be the final solution. The accuracy of the present wave model results is connected to many different factors, physical, numerical, and, of course, accuracy of the input wind fields. The impact of gustiness and a variable air density varies according to the local conditions. As we will see in the following, this impact is not necessarily larger where we find the largest errors in practical applications. Therefore, while a look at the measurements will certainly be useful, the impact must be judged with respect to a run done in the usual way, without gustiness and with a constant value of the air density.

### 5.1. Applications to the Mediterranean Sea

[40] The Mediterranean is surrounded by the rather cold Europe from the north and the rather hot Africa from the south. In this situation it is very common to have events with significant instability conditions, especially during the autumn when masses of cold air blow from north over the still warm water of the basin. The most commonly recognized examples of such conditions are the Mistral in the western part of the basin, the Bora at the northern part of the Adriatic Sea, and the northerly winds on the Aegean Sea. These cold air spills are responsible for the instability in the air-sea interaction, causing significant turbulence or wind gustiness.

[41] The hindcast period was selected to cover a continuous period of 6 months from 1 October 1993 to 31 March 1994, inclusively. This period was selected for having been very active, with storms of all kinds including Mistral and Bora. The wind and temperature data used in the experiment are the analysis surface wind  $U_{10}$ , air temperature at 2 m height,  $T_{\text{air}}$ , and sea surface temperature  $T_{\text{waters}}$ , fields resulting from the operational spectral meteorological model of ECMWF (Reading, United Kingdom). At that time the T213 version [see *Simmons*, 1991] was used, with a spectral

resolution of about 95 km. Those fields are available every 6 hours, at the major synoptic times. The standard operational WAM model was used with spatial resolution of  $0.25^\circ$  in both longitudinal and latitudinal directions.

[42] A reference run (MR, M for Mediterranean) was conducted using the wind fields without any modifications (no gustiness) to resemble the current operational conditions of the wave modeling. The gusty tests were carried out by superposing simulated gustiness over the undisturbed wind velocity in the three different ways mentioned earlier: flip-flop (MF), no-coherence (MN), and with 0.90 coherence. The coherence run was done with both 15 (MC15) and 3 min (MC03) integration time steps.

[43] Table 1 shows the  $H_s$  differences between each run and the reference one (MR) over the 6 month period. The first column gives the mean and the maximum values found in MR for a better quantification of the differences. The absolute, at any grid point at any instant, maximum gain and loss of  $H_s$  are tabulated. The ranges for the long-term mean differences (biases) are tabulated as well.

[44] The range of  $H_s$  variation of the coherence runs is rather wide. There is a tendency toward a negative effect of gustiness on the wave height values for the runs with the standard 15 min integration time step, MF, MN, and MC15, a direct consequence of the kink noticed in the single-point runs. The situation is quite different for the 3 min run MC03, where there is a clear tendency toward larger wave heights. The maximum increase of more than 1.5 m (and even 2 m for the MC03 run) indicates the possible transient effects of gustiness. The overall average differences with respect to the reference run are rather small, of the order of centimeters. This apparently low value can be misleading, as air-sea instability, hence gustiness, is not present all the time. The values represent the averages of a large majority of neutral wind or low-wind conditions and a relatively few isolated gusty events, typically happening in specific areas like the Gulf of Lion (Mistral), the northern Adriatic Sea (Bora), and the Aegean Sea.

[45] The effect of gustiness on the wind and wave climate was assessed by plotting the probability density functions of wind speed and significant wave height. Figure 5 shows these plots for the western Mediterranean Sea, including the air density effects discussed later. The logarithmic scale does not allow the perception of the intermediate values, but it shows clearly the drastic increase of the occurrence probability of the high values. The maximum wave heights are increased by more than 15%. Of course, such enhancements happen in the regions characterized by frequent high air-sea instability conditions mentioned above.

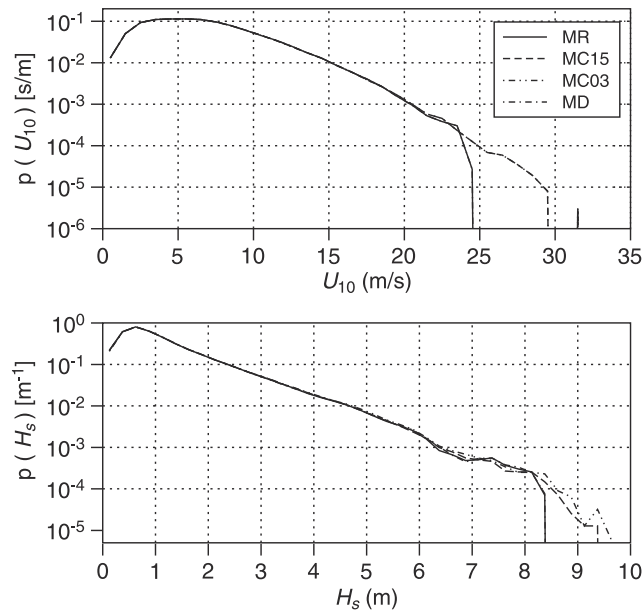


**Figure 5.** The probability density functions of wind speed and significant wave height for the western Mediterranean Sea during the 6 month period.

[46] While a single extended simulation can provide a general idea of the impact of gustiness on the climatology, its randomness does not allow definite conclusions when we focus on a specific location and on a given storm. Similar to what was done with the single point model, a better idea can be obtained with the ensemble approach, i.e., by repeating the hindcast a large number of times and analyzing the overall distribution of the results. A typical Mistral storm was selected. It had occurred between 21 and 24 October

1993, when northwesterly cold winds were blowing offshore France over the still warm waters of the western Mediterranean basin. At the storm peak during the first half of 22 October the wind speed  $U_{10}$  exceeded  $25 \text{ m s}^{-1}$ , as estimated by ECMWF meteorological model. The rather unstable air-sea conditions caused wind speed fluctuations with estimated  $\sigma$  values exceeding 0.2. Figure 6 shows the spatial distribution of  $U_{10}$ , as vectors, and  $\sigma$ , as isolines, averaged over the effective duration of 22–24 October, inclusively. The 50 hindcasts of this storm were carried out, with wind gustiness having 0.90 coherence, using for each simulation different random sequences. Figure 7 shows the results, in terms of wave height, at Alghero, located on the northwest corner of Sardinia at around  $40.5^\circ\text{N}$ ,  $8.0^\circ\text{E}$  (see Figure 6). The hatched envelope and the mean of the 50 runs, together with the reference nongusty run and the measurements, are shown in Figure 7. Except for the early stages of the storm the impact of gustiness on the wave height values is clear in that even the lower edge of the  $H_s$  envelope is almost equal to or higher than the reference curve. For this case the gustiness caused a maximum increase of the predicted wave heights of 15% at the peak of the storm. At the same time the ensemble mean was higher by 20 cm (5%).

[47] Comparing these results with those in Figure 3, it is immediately evident that in practical applications the enhancement of  $H_s$  due to gustiness does not reach the high peak values that can characterize the tests with the single-point model. There are two reasons for this. The first one is that the relatively short fetch conditions often present in the Mediterranean Sea do not allow a sufficient development of the wave system to trigger a large action of the diode effect. The second reason is that the single-point model implicitly assumes a unitary coherence in space, versus the null value we assumed for the hindcasts. Therefore it was much more unlikely to encounter in our tests an area of wind speed values, all biased in the same direction, that would lead to

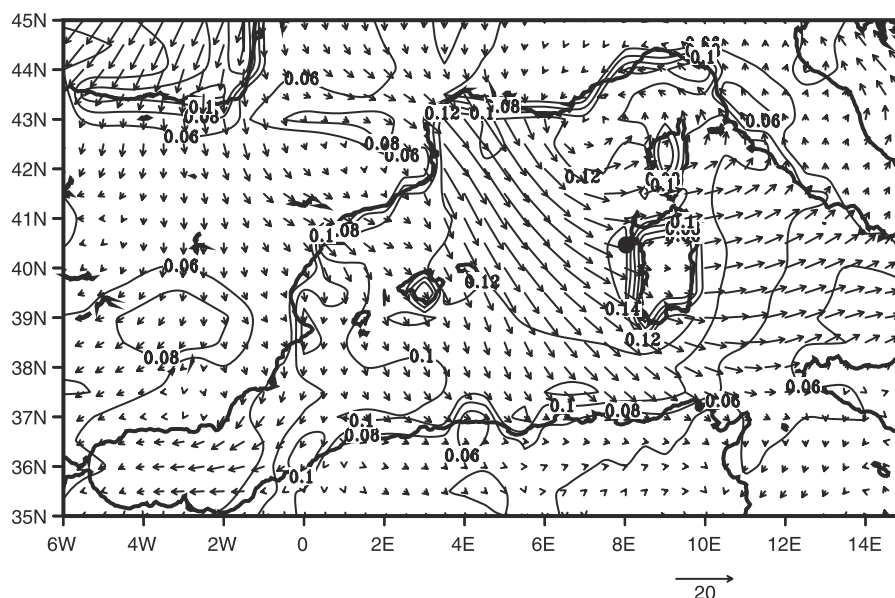


**Figure 6.** The geographical distribution of  $U_{10}$  in  $\text{m s}^{-1}$ , as vectors, and  $\sigma$ , as isolines, averaged over the period 22–24 October 1993 over the western Mediterranean Sea. Alghero gauging station is indicated by a dot.

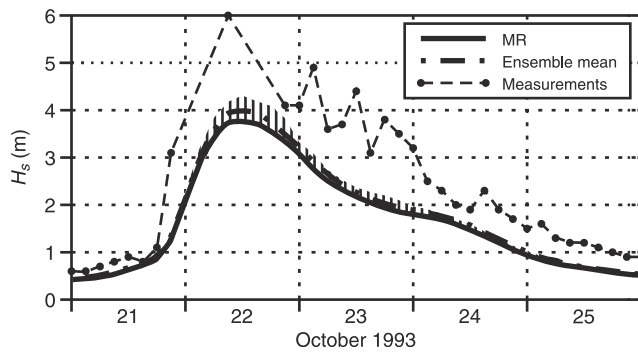


**Figure 7.** Time histories of significant wave height at Alghero (see Figure 6 for its location). The hatched area represents the ensemble envelope. MR is the reference run.

large  $H_s$  differences from the reference run. As pointed out at the beginning of this section, the implications of a finite spatial coherence will be discussed later in section 8.

[48] Another immediate deduction from Figure 7 is that although the enhancement due to gustiness is in the correct direction, it cannot justify the differences with respect to the measured values. These differences are generally attributed to the negative errors that typify the surface wind model results in enclosed basins, particularly when surrounded by a relevant orography [see *Komen et al.*, 1994; *Cavaleri and Bertotti*, 2000]. High-resolution meteorological modeling is not necessarily a solution [see, e.g., *Bertotti et al.*, 1998]. While considering gustiness can alleviate the problem, clearly, the bunch of it remains. However, it is interesting to note the oscillations in the measured  $H_s$  values, which suggest the existence of strong variability in the fields.

**5.2. Applications to the North Atlantic Ocean**

[49] The other experiment concerned the 6 month hindcast in the North Atlantic Ocean. Such an experiment was necessary to display the possible effects of wind gustiness on wave growth under longer fetch conditions than in the Mediterranean Sea. The hindcast period was selected to cover a continuous period of 6 months from 1 October 1999 to 31 March 2000, inclusively. This period represents the Northern Hemisphere winter, when the North Atlantic is particularly stormy. The wind data used in the experiment are the analysis  $U_{10}$  fields from the ECMWF meteorological model T319, operational at the time, with a spectral resolution of about 60 km. T319 is an advanced version over the previous T213. All the other details on the introduction of gustiness into the wind fields were identical to those used for the Mediterranean hindcast. The WAM model was used with spatial resolution of  $1.0^\circ$  in both latitudinal and longitudinal directions.

[50] For the purpose of wave modeling, only the part of the ocean extended from  $30^\circ$  to  $81^\circ\text{N}$  was selected, to maintain the computational resources and data storage within manageable limits. Hence a closed boundary was assumed along the latitude  $30^\circ\text{N}$ . Certainly, this had implications on the wave results, as the lack of swell from the south and incorrect results in the case of southerly winds. On the northern border the ice extension was not considered. However, as the attention was focused mainly on the differences between gusty runs and the reference one, similarly evaluated, these limitations are not expected to affect the derived conclusions. Rather, they impede a direct objective comparison with the measured data in the ocean.

[51] Similar to what was done in the Mediterranean experiment, a reference run (AR, A for Atlantic) was conducted using the wind fields without any modification. The gusty tests included the flip-flop (AF) run, the no-coherence (AN) run, and the 0.90 coherence run. The coherence run was done with both a 15 (AC15) and a 3 min (AC03) time step.

[52] Table 2 shows the  $H_s$  differences between each run and the reference run over the 6 month period, together with the mean and maximum values of each parameter obtained from the reference run. The main difference compared to the Mediterranean results is the more pronounced gain in wave height. The kink still has an impact on the results, as can be derived from the comparison of AC03 and AC15 results. The larger wave heights that characterize the North Atlantic Ocean, and the extended fetches, with a stronger action of the diode effect, enhance the effect of gustiness. This is reflected in the very large values of the maximum wave height differences, with a peak larger than 6 m. Such a large value prompted an analysis of the related wind and wave conditions. It was associated with a violent north-westerly storm blowing off the coast of the United States, south of Nova Scotia, characterized by extreme air-sea instability conditions. According to equation (4), the  $\sigma$  values were estimated to be in excess of 0.5. For an undisturbed wind speed between 16 and  $18\text{ m s}^{-1}$ , periods with values up to  $25\text{--}30\text{ m s}^{-1}$  will be relatively frequent, with the consequent enhancement of the derived wave heights.

[53] Looking again at the more limited, but still significant, average gain (point by point) over the whole hindcast, this is, of course, much more limited (see Figure 8), with most of the values comprised between 10 and 15 cm and local peaks of up to 20 cm. It is interesting to note that these gains in wave height are comparable to the present ECMWF operational wave model underestimates [*Bidlot et al.*, 2000]. The ECMWF wave model results are lower than ERS-2 altimeter wave heights by about 14 cm during the same period for the same region. The underestimate increases up to about 40 cm when the comparison is done against buoy data. This suggests that the introduction of gustiness can

**Table 2.** As Table 1 but for the North Atlantic Ocean

	AR	AF	AN	AC15	AC03	AD
Maximum negative difference, m	...	-1.20	-1.09	-2.39	-2.35	-0.49
Lowest mean, m	4.13	-0.05	-0.00	-0.00	+0.00	-0.01
Highest mean, m	4.13	+0.05	+0.07	+0.17	+0.20	+0.10
Maximum positive difference, m	14.73	+1.15	+2.37	+5.87	+6.59	1.09

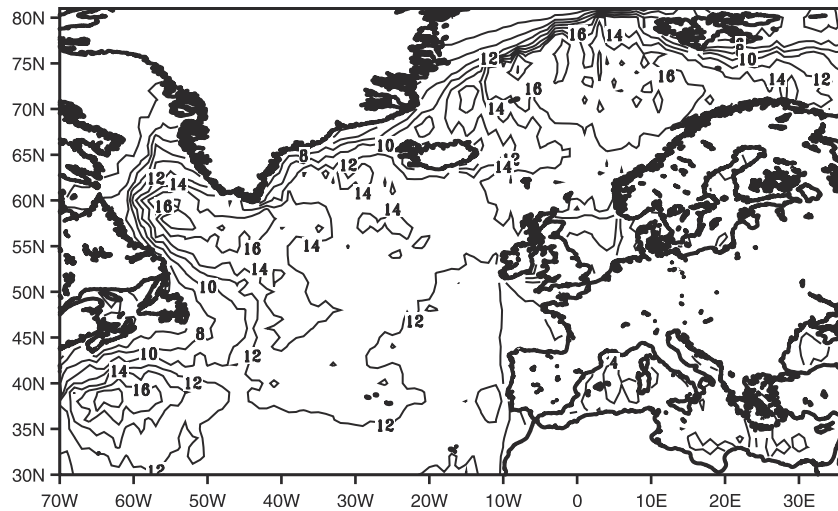


**Figure 8.** The distribution of the mean wave height differences, in centimeters, between the coherence (AC03) and the reference (AR) runs in the North Atlantic during the 6 month period.

indeed lead to a substantial improvement of the wave results in the North Atlantic.

[54] The impact on the probability density functions of wind and significant wave height is shown in Figure 9. It is clear that the wind gustiness leads to a substantial shift of the distributions toward the higher values. There is an increase of about 2 m in the maximum value of the wave height. This drastic shift appears on the whole basin, unlike the Mediterranean, where the enhancement is regional and occurs only for high values of wind speed and instability.

[55] A detailed comparison of the different hindcasts was done against the wave-measured data available at the three buoy locations shown in Figure 10. Stations 62026 (55.3°N, 2.3°E) and 62109 (57.0°N, 0.0°E) are located in the North Sea, while station 64046 (60.5°N, 5.0°W) is located in the ocean, north of the United Kingdom. These stations were chosen because they are fully, in the North Sea, or partially, north of the United Kingdom, sheltered from the southern swell, not represented in the present tests. At station 64046 the introduction of gustiness leads to a substantial reduction of the 6 month  $H_s$  bias, from  $-47$  to  $-31$  cm, the best results being obtained by the coherence run. The improvement, not so substantial, as expected, because of the randomness introduced in the forcing wind fields, is present also in the RMS error. In the North Sea the results are more neutral, consistent with the already very low bias of the reference  $H_s$ . The results from the various gusty runs are very similar, with the coherence run having a slight positive bias (a few centimeters) compared to the AR and AN runs.

[56] Similar to what was done in the Mediterranean, a particular storm was selected for an ensemble analysis of the effect of gustiness. A stormy period was selected between 15 and 20 December 1999. This period was characterized by a sustained level of gustiness in the stormy northeastern part of the Atlantic, where there were also wind and wave measurements with which to compare. This part of the ocean is mostly sheltered from the southern swell; hence a comparison between model and measured data can provide useful indications. However, the problem described earlier regarding the northern ice border still applies. During the

most active part of the storm, which was 17–19 December, over the northeastern Atlantic the wind was dominantly northwesterly, with wind speed up to  $24 \text{ m s}^{-1}$  and  $\sigma$  values around 0.2. Figure 10 shows the spatial distribution of  $U_{10}$ , as vectors, and  $\sigma$ , as isolines, averaged over the effective duration of 17–19 December. Fifty simulations of the storm, each one with different random number sequences, were carried out. A 3 day warming up period was used. The results of the 50 runs were analyzed at the three buoy locations shown in Figure 10. The results of this analysis for station 64046 are given in Figure 11, showing the significant wave heights derived from the measurements, the reference (AR) and the no-coherence (AN) runs, and the range (hatched) of the 50-run envelope and the means.

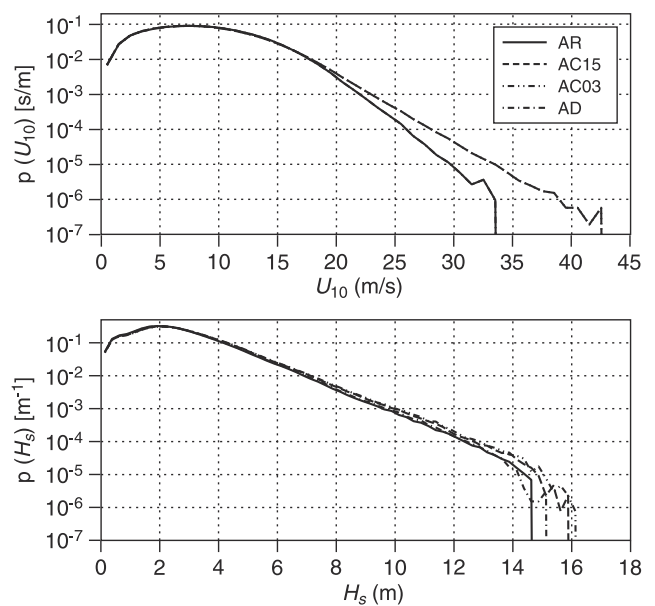


**Figure 9.** The probability density functions of wind speed and significant wave height for the North Atlantic during the 6 month period.

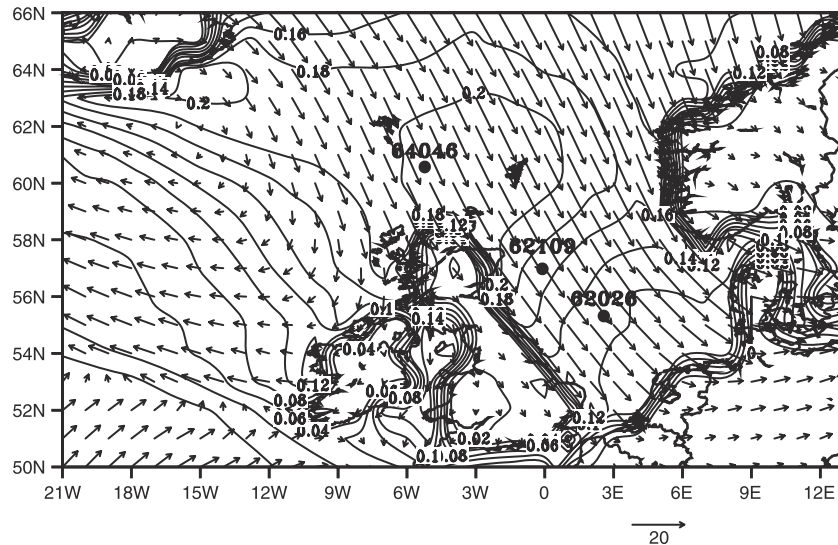


**Figure 10.** The distribution of  $U_{10}$  in  $\text{m s}^{-1}$ , as vectors, and  $\sigma$ , as isolines, averaged over the period 17–19 December 1999 over the northeastern part of the North Atlantic Ocean. The three dots indicate the locations of the buoys used for the comparison with the ensemble test.

[57] The onset of gustiness is made dramatically evident by the rapid increase of the hatched area in the early hours of 18 December. Note that the gusty runs are almost always higher (larger  $H_s$ ) than AR (compare AR with the lower border of the ensemble). There is a substantial decrease of the average negative bias (62 cm) with respect to the buoy data, down to 47 and 25 cm for the no-coherence and the ensemble mean, respectively. The flip-flop run (not shown) has results similar to AN.

[58] While Figure 11 shows the range of the possible values associated with gustiness (within the size of the ensemble), it does not provide information on the associated probability distribution. For practical applications the question is the following: granted that gustiness leads, on the average, to an increase of the significant wave heights, which is the probability, p.e., of encountering sea conditions 20% higher than the undisturbed nongusty value? Remember that we are talking about sea states, not height of individual waves. Information can be obtained by analyzing, for each available time, the distribution of  $H_s$  within the ensemble. Therefore, to reply, at least qualitatively, to the above question, we have plotted in Figure 12 the probability distributions for 14 different times at 3 hour intervals across the peak of the storm. For each instant the  $H_s$  scale has been normalized with respect to the mean of the ensemble at the same time,  $\langle H_s \rangle$ . We have then extracted an average distribution, calculated, at each point of the horizontal scale, as the mean of the 14 available values. This is plotted in Figure 12 as the thick dashed line. So, the average distribution we derive from Figure 12 tells us that at each time we have, for example, 40% probability of encountering a sea state 10% larger than the ensemble mean. The effect of gustiness is highlighted by plotting also the range of the normalized nongusty values,  $R$ , which are between 7 and 14% lower than  $\langle H_s \rangle$  (12% on average). The no-coherence run, also plotted as  $N$ , is only 4% (on average) lower than  $\langle H_s \rangle$ .

[59] It is tempting to give an analytical form to the average distribution in Figure 12. While we do not give a

theoretical basis for it, we strongly suggest that if properly adimensionalized, its basic characteristics do not depend on the specific wind speed, level of gustiness, or stage of development of the wave field. If this is indeed the case, it would be possible to derive in any wave conditions useful indications about the possible distribution of sea states associated with gustiness. The reference parameter is the gain between the undisturbed nongusty wave height  $H_o$  and the ensemble mean  $\langle H_s \rangle$ . We define the average percent increase of  $H_s$  as

$$\Delta = (\langle H_s \rangle - H_o) / H_o. \quad (5)$$

Then, on a very qualitative basis we note that most of the possible sea states have a percent increase of the significant wave height lower than  $\Delta$ . The most probable sea state is at about  $0.75\Delta$ . Here 30–40% of the cases have an increase of

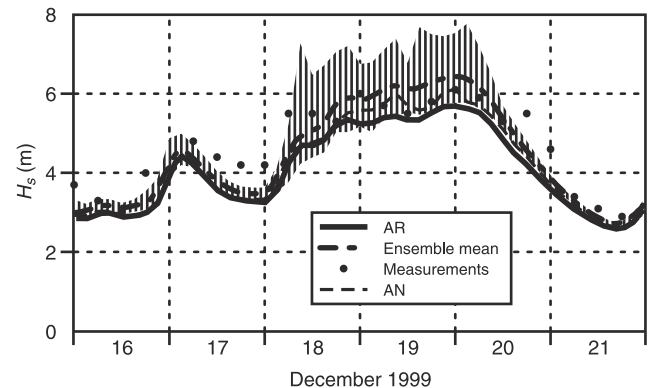


**Figure 11.** Time histories of significant wave height at buoy 64046 (see Figure 10 for its location). The hatched area represents the ensemble envelope. AR is the reference run; AN is the no-coherence run.

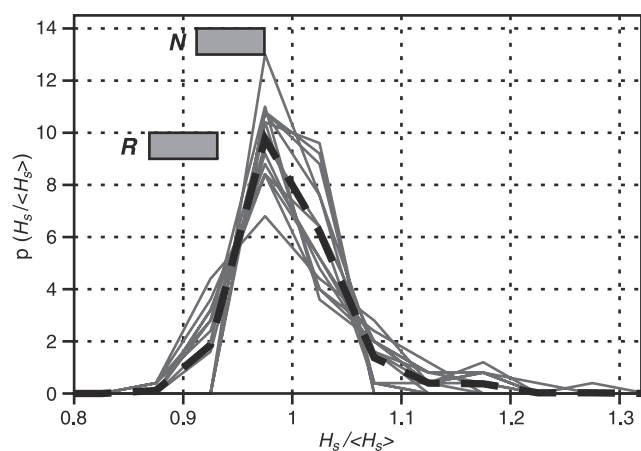


**Figure 12.** Individual distributions of significant wave heights, each normalized with respect to its own mean value  $\langle H_s \rangle$  for 14 different times in the central part of the ensemble period in Figure 11. The thick dashed line represents the average of all distributions. The two hatched areas marked as *R* and *N* show the corresponding significant wave height range obtained with the reference run and the no-coherence run, respectively.

$H_s$  larger than  $\Delta$ . In about 5% of the cases the percent increase is larger than  $2\Delta$ .

## 6. Air Density

[60] In this section we discuss the dependence of the evolution of wind waves on the density of the forcing air field, and its implications for practical wave modeling applications.

### 6.1. Air Density Variability and Its Effect

[61] The air density depends mainly on the atmospheric pressure, the air temperature, and the humidity. As these parameters vary in time and space, the air density varies as well. Nevertheless, in general, wave models do not consider this variability and assume a constant value throughout their computations. As an example, WAM assumes  $1.225 \text{ kg m}^{-3}$ . One possible reason for this handicap is that air density is not a standard product of the meteorological models and must be derived from other products, namely, atmospheric pressure and dew point temperature. The term variable air density is used here to refer to the air density computed from the meteorological model data at each grid point and each time.

[62] For a given wind speed value  $U_{10}$  the total shear stress, or vertical momentum flux  $\tau$ , in the atmosphere due to wind flow depends on the air density  $\rho_a$ . Therefore (see section 2) the wind input is linearly proportional to the air density value. A sustained increase (or decrease) in  $\rho_a$ , compared to the widely used  $1.225 \text{ kg m}^{-3}$  value, would lead to a similar increase (or decrease) in the rate of wave growth.

### 6.2. Single-Point Runs

[63] Similar to the approach followed in section 4, the single-point runs are very helpful in visualizing the impact.

The same configuration of the runs was used, with a steady wind speed of  $15 \text{ m s}^{-1}$  and integration time step of 15 min. The reference run was done with the standard value of  $\rho_a$ ,  $1.225 \text{ kg m}^{-3}$ . Runs with other constant values of  $\rho_a$  were carried out as well. Figure 13 shows the growth curves of the reference run together with runs using air densities increased and reduced by 3 and 10% with respect to the standard value.

[64] Focusing on the more evident differences associated with a 10% increase of  $\rho_a$ , we find a rapid growth of the differences, up to 25 cm, with respect to the reference run during the early phases of development. This is because at this stage the input term is the only one affected by the change of density. The later development shows almost constant  $H_s$  differences, when the other processes, for example, white capping, adapt to the new situation.

## 7. Practical Applications With Variable Air Density

[65] To assess the possible effects of using a variable air density on wave growth under real conditions, the same long-term hindcast experiments used for gustiness were repeated using the variable air-density fields. The same model setup used for the previous tests was repeated here but without gustiness effects. The air density values were derived from those of atmospheric pressure, air temperature, and humidity, extracted from the ECMWF archive.

### 7.1. Applications to the Mediterranean Sea

[66] The reference run (MR) with the standard  $\rho_a$  value of  $1.225 \text{ kg m}^{-3}$  was the same one used for the gustiness tests. Another run was carried out using the proper  $\rho_a$  fields (MD run). The differences between the MD and MR runs over the whole period of 6 months are tabulated as the last column in Table 1. On average, considering the air density variability leads to wave height variations of  $<1 \text{ cm}$ . This is because, in general, the air density in the Mediterranean does not differ much from the standard value, varying mostly between  $1.16$  and  $1.24 \text{ kg m}^{-3}$ . However, instantaneous  $H_s$  differences as high as 37 cm are possible. On the

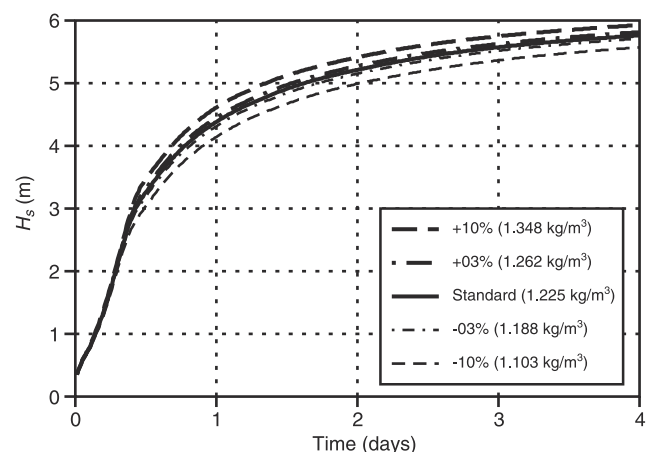


**Figure 13.** Effect of different values of air density on the significant wave height growth curves from single-point runs.

overall basin most of these values vary between 6 and 8 cm. Expectedly, the localized relatively large positive differences are typically associated with northerly flows of cold air, particularly when the Azores high-pressure zone, **H**, is extending over central Europe, following a deep low, **L**. In these conditions, strong pressure gradients are present at the border between the two zones. The areas just under the influence of **H** experience strong high-density winds, leading to the largest increases with respect to a reference run with a constant density. As for gustiness, the three areas prone to such situations are the northern part of the western Mediterranean Sea (Mistral), the northern part of the Adriatic Sea (Bora), and the northern part of the Aegean Sea.

[67] The dependence of wave climate on the use of a variable air density was also examined through the impact on the probability density function of the wave height as shown for the western Mediterranean Sea in Figure 5. There is virtually no change in the  $H_s$  distribution. When the whole basin is considered (not shown), there is a slight reduction in the highest  $H_s$  conditions. This can be explained by the fact that most storms occur as a result of low-pressure conditions. The low-pressure indeed causes a reduction of air density, which in turn, leads to reduction in the wave growth.

### 7.2. Applications to the North Atlantic Ocean

[68] As before, the reference run AR was the same one used for the gustiness tests. The differences between the density run AD and AR over the whole period of 6 months are tabulated as the last column in Table 2. On average the air-density variability results in wave height biases not exceeding 10 cm when compared to the reference run. However, instantaneous reductions as large as 50 cm and increases as high as 1.1 m were found. The air density in the North Atlantic is generally higher than the standard value and varies mostly between 1.1 and 1.5 kg m<sup>-3</sup>. This leads to a distributed limited, but always positive, increase of  $H_s$  throughout the basin. It is instructive that the largest average increases happen in the most northerly areas, east of Greenland, and in the Baffin Bay, where there are frequent inflows of cold dense air from the North. A similar argument applies to Figure 14, which shows the maximum positive and negative  $H_s$  differences for the whole grid associated with the use of fields derived with variable air density. There are two clearly distinct distributions. The positive values are mainly located at high latitudes. The opposite is true for the negative differences associated with the inflow of warm air from the south. Similarly, the average  $H_s$  differences throughout the period tend to increase from south to north (not shown).

[69] A similar analysis for the wave climate shows (see Figure 9) a marginal enhancement in the distribution of wave heights, with the large  $H_s$  values being slightly higher than those produced with the standard  $\rho_a$  value. The same results were found for almost all the individual regions, except for some of the interior basins. This is consistent with the results of the single-point run in section 6.2.

### 7.3. Combined Gustiness/Density Run

[70] As a final test, we have done a run introducing both the gustiness, following the procedure described in section 5, and a variable air density. The test has been done for the North Atlantic, the one of the two considered areas where

the effects are stronger. The same storm used for the ensemble has been considered.

[71] The results are reported in Figure 15 for buoy 64046 (see Figure 10 for its location). Here we show differences, with respect to the reference run (no gustiness and constant air density), of the runs done with only gustiness (GE), only variable air density (DE), and the combination of both (continuous line). The relevant point is that the combined effect is larger than the sum of the two separate contributions (GE + DE). The difference, 10 cm at most at this location and for this storm, is indicative of the nonlinearity of the process. Our interpretation is that the increased air density implies a larger wind input to waves, which in turn, leads to an enhancement of the effect of gustiness.

## 8. Discussion

### 8.1. Gustiness Already Included in the Wind Input Term

[72] The present formulations of wind input to waves are based on theoretical arguments and substantial evidence from devoted campaigns. If gustiness is, at different levels, a permanent component of the surface wind fields, it is possible to argue that its effects should already be embedded in the formulations. This can be partly true. However, the typical reference measurements of wave growth have been obtained under fetch-limited conditions, when the differences with respect to the steady wind case are quite limited. Besides, low levels of gustiness  $\sigma$ , the most common situation encountered in the fields, have little impact on wave growth. Indeed, the effects grow very rapidly with the value of  $\sigma$  [see *Komen et al.*, 1994, p. 322], and the average long-term effects are mostly due to only part of the events, characterized by a significant gustiness. This suggests that the effects already embedded in the formulations are quite limited, and therefore it is meaningful to take gustiness into account in the practical applications.

### 8.2. Where to Expect Gustiness Effects

[73] Of the three mechanisms that contribute to the overall effect two of them, the nonlinearity of  $u^*$  on  $U_{10}$  and that of Miles mechanism on  $u^*$ , are active from the early stages of development. The most effective one, the diode effect, associated with the nonsymmetrical behavior of waves travelling faster or slower than wind speed, becomes effective only at a later stage. It follows that the overall enhancement of wave growth is limited in the early stages, growing rapidly as soon as the waves are sufficiently developed, i.e., when the phase speed of some energetic components of the spectrum becomes comparable to the wind speed. Therefore we must expect limited effects in the smaller basins, where the waves are mostly young, and larger effects in the open oceans, where the large distances allow a mature development of the storms, with the consequent enhancement of the gustiness effects. We have verified this in the Mediterranean Sea and the North Atlantic Ocean, respectively.

### 8.3. Comparison With Measured Data

[74] The intrinsic randomness present in gustiness does not allow a direct objective comparison with measured data. This can be done only in statistical terms. Another reason

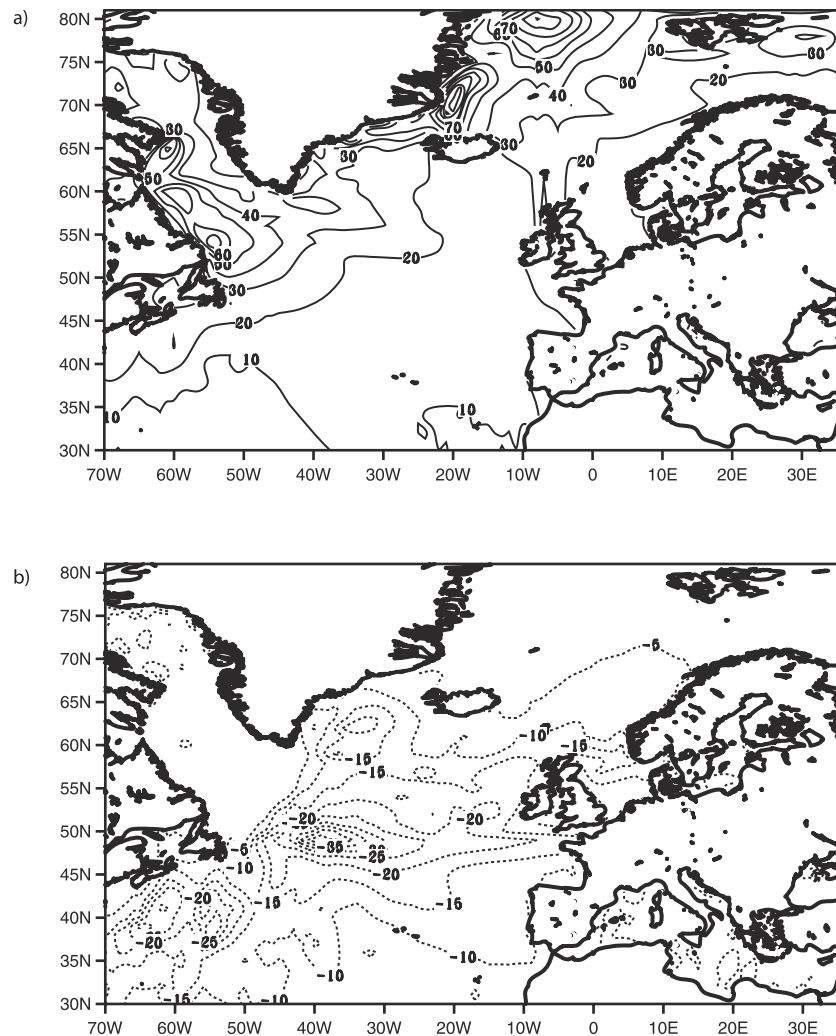


**Figure 14.** The distribution of the maximum (a) positive and (b) negative wave height differences, in centimeters, between the correct air density (AD) and reference (AR) runs in the North Atlantic during the 6 month period.

are the limitations intrinsic in our long hindcasts. In the North Atlantic the chosen border of the computational grid at 30°N and the lack of consideration for the ice extent have introduced serious errors in the computation. Nevertheless, by comparing our results to a reference run (no gustiness and constant air density) and using the performance statistics of ECMWF, we have been able to get a fair idea of the possible improvements. The operational products of ECMWF indicate a negative bias of the significant wave height of about 14 cm when compared to altimeter data and of 40 cm when compared to buoy data (for the same area and period of our hindcast). Therefore increases of 10–15 cm (gustiness) and up to 10 cm (air density) represent a drastic improvement of the model results.

[75] In the Mediterranean the results are less significant because of the limited effects of gustiness (limited fetches) and air density (typically equal to or lower than the nominal value). On top of this the wave model results are generally strongly underestimated, the accepted reason being the lack of strength in the forcing wind fields. Therefore our results, although in the right direction, are not the solution of the specific local problem, typical of all the enclosed basins.

#### 8.4. Probability of Extremes

[76] The presence of gustiness implies the possibility of higher extreme sea states. In highly unstable air-sea conditions, increases of several meters are possible. An estimate of the related statistics has been obtained with the ensemble technique by repeating the hindcast for the same period a large number of times, each one with a different realization of gustiness but always using the same  $\sigma$ . From this we have derived an average distribution of the possible significant wave heights at a certain time. The  $H_s$  range of this distribution depends on the undisturbed height  $H_0$  and on the mean enhancement due to gustiness. We suggest that properly adimensionalized, this distribution holds for any condition, providing an effective way to estimate the encounter probability of given significant wave heights.

#### 8.5. Practical Applications

[77] This leads to the subject of practical applications. An ensemble approach is not feasible in routine forecasts. On the other hand, following the arguments given in section 8.4, what we need to estimate the distribution is the undisturbed

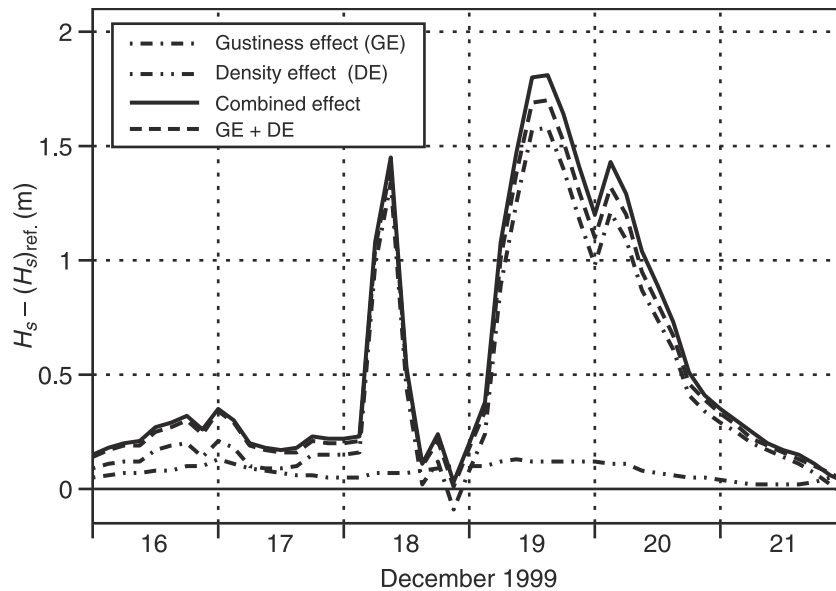


**Figure 15.** Time histories of significant wave height differences resulting from runs with only wind gustiness (GE), only variable air density (DE), and both the processes acting at the same time. The results are shown at the location of buoy 64046 in Figure 10. The summation of the differences GE and DE is also plotted for comparison. The reference run AR is shown in Figure 11.

significant wave height  $H_o$  and its difference with respect to the ensemble mean  $\langle H_s \rangle$ , i.e., the horizontal scale of the distribution in Figure 12. Lacking  $\langle H_s \rangle$ , we can use the output of the no-coherence run. From Figure 12 we see that the corresponding  $H_s$  value, say  $H_{AN}$ , is between  $H_o$  and  $\langle H_s \rangle$ . More exactly, the analysis of the ensemble results suggests  $\langle H_s \rangle - H_o = 1.5(H_{AN} - H_o)$  (within  $\pm 10\%$ ). Combined with equation (5), this provides the required estimate of  $\Delta$  as

$$\Delta = 1.5(H_{AN} - H_o) / H_o.$$

[78] On the whole we suggest the use of two runs, one without gustiness and the other one with no-coherence gustiness. Their combination provides an estimate of the probability distribution of significant wave heights at each grid point and each time.

### 8.6. Coherence in Space

[79] While the temporal coherence has been introduced into the gustiness simulation, no spatial coherence has been considered. This was due to the decrease of the spatial coherence with distance and to the large grid step we used for our most significant results. This choice implied that the wind oscillations at the single grid points were independent of each other and therefore less likely to reach high (or low) values at the same time, which would have enhanced the variability of the resulting wave field. The opposite example is given by the single-point runs, where we have implicitly assumed a spatially uniform ocean, which drastically increased the range of the extremes. The real world, with a finite coherence in space, lies between these two approaches, most likely toward our hindcasts. Therefore the latter ones should be looked at as lower limits of the extremes that can be encountered in a gusty sea.

### 8.7. Representation of Gustiness

[80] All our results are dependent on the representation we chose for gustiness. However, the algorithm we used provides time series consistent with the data available in the literature and derived from open sea measurements. Therefore, while different algorithms are possible, we do not expect the derived results to be substantially different from the present ones. More critical is the evaluation of the gustiness level  $\sigma$ . The practical problem is that the values of  $\sigma$  derived from theory [e.g., *Panofsky and Dutton, 1984*] do not justify the values encountered in the sea. Therefore we have resorted to the use of an empirical relationship between  $\sigma$  and the air-sea temperature difference derived from measurements at an oceanographic tower. As the two temperatures, air and sea, are part of the standard data of a meteorological model, this provides a practical approach to the problem. Also, the possible errors in their estimates, typically  $0.5^\circ$  for the sea surface and  $1^\circ$  for the temperature of the lowest atmospheric layer, are not significant enough to modify the conclusions.

### 8.8. Higher-Frequency Gustiness

[81] An implicit assumption in all our runs, generally accepted in wave modeling, is that the wind speed is constant along each integration time step  $\Delta t$ . This corresponds to neglecting the higher-frequency wind components. The implications have been analyzed by *Cavaleri and Burgers [1992]* and the left out energy, for  $\Delta t = 20$  min, estimated at 20%. This would correspond to an actual value of  $\sigma$  equal to 1.1 times the one used. *Janssen [1986]* proposed a way to take the shorter oscillations into account. Another interesting approach until the subwavelength scale has been recently suggested by *Miles and Ierley [1998]*. However, the relevance of the more rapid oscillations decreases when  $\Delta t$  decreases. In our case, having used

time steps as low as 3 min, at this lower limit the implications of a constant  $U$  during each integration step become negligible.

### 8.9. Air Density

[82] The use of a variable air density is rather straightforward and does not present particular problems. It is interesting to note that although the changes of wind input are generally limited, the consequences are not. This is associated with the strong spatial coherence of the air density data (large areas with the same characteristics) and the consequent reaction of the system. In this sense the single-point tests are here much more significant for practical results than the gustiness tests.

## 9. Conclusions

[83] Summarizing, the following conclusions can be drawn from the overall study.

1. Wind gustiness can be conveniently represented as a time coherent random noise; the wind characteristics so obtained are consistent with the ones derived from measured data.

2. Gustiness enhances the wave height, larger values of it leading, on the average, to much larger increases of wave height.

3. Because of coherence in time, the oscillations present in the wind fields lead to similar, but reduced, oscillations of wave height, with values much larger than in the case of no-coherent gustiness.

4. For a given wind speed the level of gustiness can be related to the air-sea temperature difference. A more theoretical evaluation of it will be welcome but is not expected to change the basic results of the present study.

5. The implications of gustiness in the Mediterranean Sea, or more generally, in enclosed basins, are limited because of dominant fetch-limited conditions. Occasional peaks are associated to the randomization of the field.

6. The implications are much larger in the Atlantic, or more generally, in open oceans. The increase of the average wave heights is comprised between 10 and 20 cm. Individual enhancements, in space and time, can go up to a few meters, or typically, 30–40% of the nongusty values.

7. The long-term statistical distribution of  $H_s$  is only marginally affected in the Mediterranean Sea; the results are more substantial in the Atlantic, with an evident shift toward higher values and a substantial reduction of the model bias with respect to measured data.

8. The statistics of the possible significant wave heights  $H_s$  at each time and location can be explored with the ensemble technique. As this is not suitable for practical applications, we suggest the use of two runs, without and with no-coherence gustiness. Combined with the derived general adimensional distribution for  $H_s$ , these two results provide an estimate of the overall statistics.

9. Coherence in space has not been considered. Its inclusion will lead to a further increase of the resulting wave heights.

10. Considering a variable air density, as estimated from the output of a meteorological model, leads to only minor effects in the Mediterranean. Changes are more substantial

in the Atlantic, with time-averaged increases of  $H_s$  up to 10 cm, with individual peak values above 1 m.

11. The combined consideration of both air density and gustiness leads to an enhancement of wave heights larger than the addition of the two separate effects.

## Notation

$a$	a randomly generated sequence with Gaussian distribution.
$b$	a simulated sequence of numbers.
$c$	wave phase speed, $\text{m s}^{-1}$ .
$f$	frequency, $\text{s}^{-1}$ or $\text{h}^{-1}$ .
$F(f, \theta)$	two-dimensional spectrum, $\text{m}^2 \text{s}$ .
$H_o$	undisturbed, nongusty wave height, m.
$H_s$	significant wave height, m.
$\langle H_s \rangle$	mean significant wave height in the ensemble, m.
$t$	time.
$T_{\text{air}}$	air temperature, $^{\circ}\text{C}$ .
$T_{\text{water}}$	water temperature, $^{\circ}\text{C}$ .
$u^*$	friction velocity, $\text{m s}^{-1}$ .
$U$	generic wind speed, $\text{m s}^{-1}$ .
$U_{10}$	wind speed at 10 m height, $\text{m s}^{-1}$ .
$\langle U_{10} \rangle$	mean (undisturbed) $U_{10}$ value, $\text{m s}^{-1}$ .
$\alpha$	coherence coefficient between sequential wind speed values.
$\gamma$	growth rate of $F(f, \theta)$ spectrum.
$\Delta$	average percent increase of $H_s$ .
$\Delta T$	$T_{\text{water}} - T_{\text{air}}$ , $^{\circ}\text{C}$ .
$\Delta t$	integration time step, s.
$\rho_a$	air density, $\text{kg m}^{-3}$ .
$\rho_w$	water density, $\text{kg m}^{-3}$ .
$\phi$	the angle between wind and wave propagation directions, degrees.
$\theta$	wave direction, degrees.
$\sigma$	$\sigma_u / \langle U_{10} \rangle$ .
$\sigma_a$	standard deviation of the sequence $a$ .
$\sigma_b$	standard deviation of the sequence $b$ .
$\sigma_u$	standard deviation of $U_{10}$ , $\text{m s}^{-1}$ .

[84] **Acknowledgments.** All the meteorological data used for this study have been retrieved from the archive of the European Centre for Medium-Range Weather Forecasts. The discussions with Peter Janssen and Anton Beljaars have been useful in highlighting various aspects of the problem. Jean Bidlot provided the buoy data used for comparison in the Atlantic ensemble exercise. Meteo France made available the TOPEX altimeter data. The buoy wind data have been retrieved from the Web site of NOAA. This work was done during a 6 month permanence of Saleh Abdalla at the Istituto Studio Dinamica Grandi Masse, in Venice, supported by the European Community Mast Project Eurowaves, CT97-0109. The work was also supported by the RTP 10.10 Western European Union Project WW-Medatlas.

## References

- Bauer, E., and R. Weisse, Determination of high-frequency wind variability from observations and application to North Atlantic wave modeling, *J. Geophys. Res.*, 105, 26,179–26,190, 2000.
- Bertotti, L., L. Cavaleri, P. De Girolamo, L. Franco, and S. Magnaldi, Hindcast and forecast of the Parsifal storm, *Il Nuovo Cimento Soc. Ital. Fis. C*, 21, 281–298, 1998.
- Bidlot, J., D. J. Holmes, P. A. Wittmann, R. Lalbeharry, and H. S. Chen, Intercomparison of the performance of the operational wave forecasting systems with buoy data, *Tech. Memo. 315*, 46 pp., Eur. Cent. for Med. Range Weather Forecasts, Reading, U. K., 2000.
- Box, G. E. P., and G. M. Jenkins, *Time Series Analysis, Forecasting and Control*, 553 pp., Holden-Day, Boca Raton, Fla., 1970.

- Cavaleri, L., The oceanographic tower *Acqua Alta*—Activity and prediction of sea states at Venice, *Coastal Eng.*, 39, 29–70, 2000.
- Cavaleri, L., and L. Bertotti, Influence of land on the modelled marine surface wind fields, *ISDGM Rep. 00-14*, 27 pp., Ist. Studio Din. Grandi Masse, Venice, Italy, 2000.
- Cavaleri, L., and G. Burgers, Wind gustiness and wave growth, *KNMI-Preprints 92-18*, 38 pp., Koninklijk Ned. Meteorol. Inst., De Bilt, Netherlands, 1992.
- Cavaleri, L., L. Bertotti, M. Hortal, and M. Miller, Effect of reduced diffusion on surface wind and wave fields, *Mon. Weather Rev.*, 125, 3024–3029, 1997.
- Freilich, M. H., and D. B. Chelton, Wavenumber spectra of Pacific winds measured by the Seasat scatterometer, *J. Phys. Oceanogr.*, 16, 741–757, 1986.
- Hasselmann, K., On the non-linear energy transfer in a gravity-wave spectrum, part 1, General theory, *J. Fluid Mech.*, 12, 481–500, 1962.
- Hasselmann, K., On the spectral dissipation of ocean waves due to white capping, *Boundary Layer Meteorol.*, 6, 107–127, 1974.
- Hasselmann, K., et al., Measurements of wind-wave growth and swell decay during the Joint North Sea Wave Project (JONSWAP), *Dtsch. Hydrogr. Z.*, 8, Suppl. A, 95 pp., 1973.
- Hasselmann, S., K. Hasselmann, J. H. Allender, and T. P. Barnett, Computations and parameterizations of the nonlinear energy transfer in a gravity-wave spectrum, part 2, Parameterization of the nonlinear energy transfer for application in wave models, *J. Phys. Oceanogr.*, 15, 1378–1391, 1985.
- Hersbach, H., and P. A. E. M. Janssen, Improvement of the short-fetch behaviour in the wave ocean model (WAM), *J. Atmos. Oceanic Technol.*, 16, 884–892, 1999.
- Jacob, C., et al., The IFS cycle CY21r4 made operational in October 1999, *ECMWF Newsl.*, 87, 2–8, 2000.
- Janssen, P. A. E. M., On the effect of gustiness on wave growth, *KNMI Afdeling Oceanografisch Onderzoek Memo 00-86-18*, 17 pp., Koninklijk Ned. Meteorol. Inst., De Bilt, Netherlands, 1986.
- Janssen, P. A. E. M., Quasi-linear theory of wind generation applied to wave forecasting, *J. Phys. Oceanogr.*, 22, 1600–1604, 1991.
- Janssen, P. A. E. M., P. Lionello, M. Reistad, and A. Hollingsworth, Hindcasts and data assimilation studies with the WAM model during the Seasat period, *J. Geophys. Res.*, 94, 973–993, 1989.
- Komen, G. J., K. Hasselmann, and S. Hasselmann, On the existence of a fully developed windsea spectrum, *J. Phys. Oceanogr.*, 14, 1271–1285, 1984.
- Komen, G. J., L. Cavaleri, M. Donelan, K. Hasselmann, S. Hasselmann, and P. A. E. M. Janssen, *Dynamics and Modelling of Ocean Waves*, 532 pp., Cambridge Univ. Press, New York, 1994.
- Makin, V. K., and V. N. Kudryavtsev, Coupled sea surface-atmosphere model, part 1, Wind over waves coupling, *J. Geophys. Res.*, 104, 7613–7623, 1999.
- Miles, J. W., On the generation of surface waves by shear flows, *J. Fluid Mech.*, 3, 185–204, 1957.
- Miles, J., and G. Ierley, Surface-wave generation by gusty wind, *J. Fluid Mech.*, 357, 21–28, 1998.
- Monahan, H. H., and P. Armendariz, Gust factor variations with height at atmospheric stability, *J. Geophys. Res.*, 76, 5807–5818, 1971.
- Munn, R. E., *Descriptive Micrometeorology*, 245 pp., Academic, San Diego, Calif., 1966.
- Panofsky, H. A., and J. A. Dutton, *Atmospheric Turbulence*, 397 pp., John Wiley, New York, 1984.
- Ponce, S., and F. J. Ocampo-Torres, Sensitivity of a wave model to wind variability, *J. Geophys. Res.*, 103, 3179–3201, 1998.
- Sethuraman, S., Atmospheric turbulence and storm surge due to Hurricane Belle (1976), *Mon. Weather Rev.*, 107, 314–321, 1979.
- Simmons, A., Development of the operational 31-level T213 version of the ECMWF forecast model, *ECMWF Newsl.*, 56, 3–13, 1991.
- Smith, S. D., K. B. Kataros, W. A. Oost, and P. G. Mestager, Two major experiments in the Humidity Exchange Over the Sea (HEXOS) program, *Bull. Am. Meteorol. Soc.*, 71, 161–172, 1990.
- Snyder, R. L., F. W. Dobson, J. A. Elliott, and R. B. Long, Array measurements of atmospheric pressure fluctuations above surface gravity waves, *J. Fluid Mech.*, 102, 1–59, 1981.
- Tournadre, J., and S. Blanquet, Wind speed and wave mesoscale variability from in situ and altimeter data, *Global Atmos. Ocean Syst.*, 2, 221–245, 1994.
- WAMDI Group, The WAM model—A third generation ocean wave prediction model, *J. Phys. Oceanogr.*, 18, 1775–1810, 1988.

---

S. Abdalla, European Centre for Medium-Range Weather Forecasts, Reading RG2 9AX, UK. (abdalla@ecmwf.int)

L. Cavaleri, Istituto Studio Dinamica Grandi Masse, S. Polo 1364, 30125 Venice, Italy. (L.Cavaleri@isdgm.ve.cnr.it)